



Interfaces Reduce Dislocation Loop Formation in Irradiated Nanolayered Zr-2.5Nb

Jie-Wen Zhang, Si-Mian Liu, Wei-Zhong Han*

Center for Advancing Materials Performance from the Nanoscale, State Key Laboratory for Mechanical Behavior of Materials, Xi'an Jiaotong University, Xi'an 710049, People's Republic of China



ARTICLE INFO

Article history:

Received 25 January 2021

Revised 11 March 2021

Accepted 24 March 2021

Available online 7 April 2021

Keywords:

Interface

Irradiation

Dislocation loop

Zr-2.5Nb

ABSTRACT

Interface engineering is a useful method to reduce the accumulation of irradiation defects in metals. Here, we study the effect of interface on the formation of dislocation loops in helium and krypton ions irradiated nanolayered Zr-2.5Nb. Nanolaminated α/β -Zr duplex-phase structures remain stable after irradiation at 400 °C up to 20 dpa. Dislocation denuded zones with width of 30 to 40 nm are formed at interfaces. The number density and size of both a-loops and c-loops are smaller in nanolayered sample because of interface accelerating point defects recombination. These observations indicate that α/β -Zr interfaces effectively reduce dislocation loops formation.

© 2021 Acta Materialia Inc. Published by Elsevier Ltd. All rights reserved.

Zirconium (Zr) alloys are widely used in nuclear reactor as pressure vessels and fuel claddings because of small thermal neutron capture cross-section, excellent corrosion resistance and high temperature mechanical properties [1,2]. Servicing in nuclear reactor, Zr alloys are exposed to high energy neutron irradiation, which induces a large number of self-interstitials and vacancies. These point defects further diffuse, coalesce at preferred crystallographic planes, and eventually evolve into two types of dislocation loops, a-loops with Burgers vector of $1/3<11\bar{2}0>$ and c-loops with Burgers vector of either $1/2<0001>$ or $1/6<20\bar{2}3>$ [3-11]. The a-loops, forming by the coalescence of either interstitials or vacancies, appear immediately on prismatic plane {1010} even at low irradiation dose [3-9], while the formation of c-loops within basal plane requires a critical irradiation damage [9-11]. Unfortunately, the accumulations of both a-loops and c-loops are origin for undesired irradiation hardening [4,5,12] and anisotropic irradiation growth in Zr alloys [13-15]. Therefore, reducing irradiation-induced dislocation loops is crucial in improving the irradiation tolerance of Zr alloys.

Interface engineering is a useful method to design radiation-tolerant structural materials [16-21]. Interfaces, such as grain boundaries and phase interfaces, are efficient sinks to accelerate the recombination of irradiation-induced point defects [16-21]. Self-interstitials can also be re-emitted from interface and then annihilate with vacancies nearby. As a result, self-interstitials and vacancies recombination rates can be significantly enhanced, leav-

ing a healed crystal, especially in the vicinity of interface [22,23]. These mechanisms are supported by the formation of defect-denuded zones near interfaces and the reduced irradiation defects density in irradiated nanostructured materials [17-21].

To exploit the concept of interface engineering, several methods have been developed to fabricate interface-dominant Zr-based composites [24-27], but these methods are difficult to be advanced to industrial scales and have potential contaminations during fabrication. Besides, the nanocrystalline metals become unstable and coarsen rapidly under irradiation at even modest temperature conditions [28]. To avoid above-mentioned drawbacks, a dynamic thermal-mechanical phase transformation (DTMPT) method was designed to fabricate hierarchical 3D nanolayered Zr-2.5Nb alloy in a recent study [29]. Owing to numerous 3D randomly oriented nanoscale α/β bi-phase interfaces, this novel Zr-2.5Nb has good combination of strength, strain hardening, and ductility [29]. Meanwhile, the nanolayered Zr-2.5Nb is thermally stable till to 700°C [30]. However, the efficiency of α/β interface in suppressing irradiation-induced defect still remains unclear.

Ion irradiation has been commonly recognized as a substitute with high efficiency to explore neutron irradiation damage under standard laboratory conditions [6,31-33]. Similar with neutron irradiation experiments, materials irradiated by high energy ions also experience primary knock-on atom, displacement cascade and point defects diffusion, producing comparable irradiation defects [31-33]. Compared with neutron irradiation, ion irradiation shows considerable advantages, such as higher damage rate, little or no residual radioactivity, shorter experiment period, lower cost and more precise parameter control [6]. Thus, ion irradiation is conve-

* Corresponding author.

E-mail address: wzhanxjtu@mail.xjtu.edu.cn (W.-Z. Han).

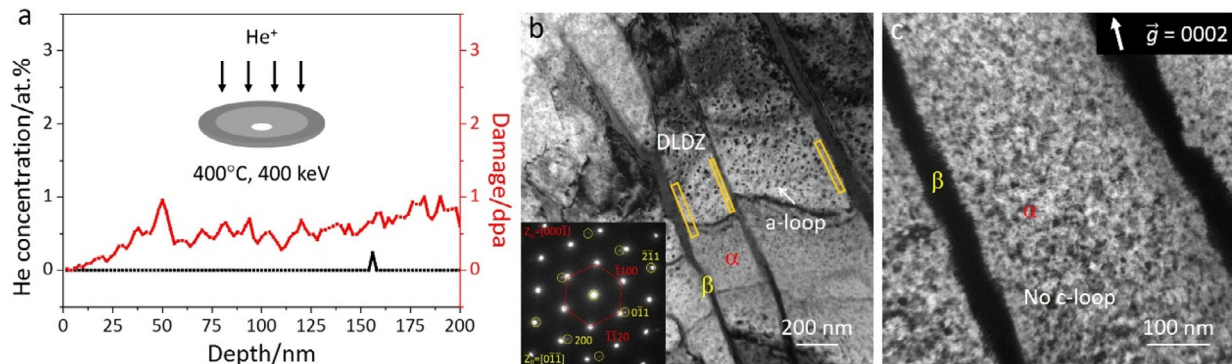


Fig. 1. (a) Depth-dependent irradiation damage (red line) and He concentration (black line) in nanolayered Zr-2.5Nb. (b) Microstructures of He-irradiated nanolayered Zr-2.5Nb. DLDZ for dislocation loop denuded zone. (c) No c-loops in He irradiated nanolayered Zr-2.5Nb.

nient to evaluate the effect of α/β interfaces on irradiation damage in nanolayered Zr-2.5Nb.

In this study, we performed helium (He) and krypton (Kr) ion implantation on hierarchical 3D nanolayered Zr-2.5Nb alloy with a high density of α/β interfaces. For comparison, pure Zr is also irradiated under the same conditions. Dislocation loop denuded zone (DLDZ), number density, size and types of a-loops and c-loops were analyzed using transmission electron microscope (TEM). We show that, in contrast to pure Zr, profuse α/β interfaces give rise to higher irradiation resistance via accelerating interstitials-vacancies recombination, making nanolayered Zr-2.5Nb alloy a promising structural materials for irradiation environment.

Hierarchical 3D nanolayered Zr-2.5Nb was fabricated by DTMPT method [29]. The alternating α -Zr and β -Zr lamellae are located within a single colony and have a classical Burgers orientation relationship of $[0001]||[011]$, $(\bar{1}120)||(\bar{1}\bar{1}1)$ and $(\bar{1}100)||(\bar{2}\bar{1}1)$. The α -Zr lamella thickness distributes in a wide range, and varies from 100 nm to 700 nm, with an average layer thickness of 222 nm, while the β -Zr lamella thickness is only 20 nm [29]. TEM foils of nanolayered Zr-2.5Nb alloy and pure Zr were prepared by mechanical grinding and twin-jet polishing [11,29]. To characterize irradiation-induced dislocation loops without interference from any implanted ions, TEM foils were irradiated by 400 keV He ions at 400°C to a dose of 1×10^{17} ions/cm² (corresponding to a dpa rate of 1.19×10^{-4} dpa/s). According to the Stopping and Range of Ions in Matter simulation using full cascade damage mode and an average displacement energy of 40 eV for pure Zr, the concentration of He in the 200 nm TEM foil is zero and the average irradiation damage is about 0.5 dpa (Fig. 1(a)). Thus, the incident He ions can entirely pass through the electron-transparent regions of TEM foils, and the effect of residual He ions on dislocation loop formation is negligible. Kr ion irradiation was also performed to explore the effect of interfaces on c-loop formation at 400°C to a dose of 5×10^{15} ions/cm². The average damage in TEM foil is about 20 dpa after Kr implantation [11]. The typical regions of the TEM foils used to characterize radiation defects have a uniform thickness in the range of 100 nm to 150 nm.

Figures 1(b) and (c) show TEM images of nanolayered Zr-2.5Nb after He ion irradiation. The nanolayered duplex-phase structure remains stable, and no new phase precipitates from both α -Zr and β -Zr lamella. According to the selected area diffraction patterns (SADP) inserted in Fig. 1(b), the Burgers orientation relationship is maintained between adjacent α/β -Zr phase. Meanwhile, the α/β interface is still near prismatic plane ($\bar{1}100$) of the α -Zr phase and ($\bar{2}\bar{1}1$) plane of the β phase [29]. However, a large number of small dislocation loops can be detected within α -Zr lamella, as labelled by the white arrows in Fig. 1(b). Because a slight misorientation inevitably exists in α -Zr lamella, some dislocation loops away from

the centre show a weak contrast. Distinct DLDZ are present in the vicinity of α/β interface, as marked by the orange rectangles in Fig. 1(b). The appearance of DLDZ hints that the α/β interfaces are able to heal irradiation damage, and thus achieve a better irradiation stability. In order to determine the Burgers vector of these dislocation loops, several α -Zr lamellae were analysed under a strict two-beam condition. Under $\vec{g} = 0002$, as shown in Fig. 1(c), no c-loops and only a-loops form under He irradiation to about 0.5 dpa. In general, the formation of c-loops requires a critical irradiation damage of 3 dpa [11].

Figure 2 displays a-loops formed in the irradiated pure Zr and α -Zr lamellae with different lamellae thickness. α -Zr lamellae were selected within a single colony to ensure the same He ion incident direction, α/β interface orientation and sample orientation. All these a-loops were observed under a two-beam condition of $\vec{g} = 10\bar{1}1$ with zone axis close to $[11\bar{2}3]$. A high density of a-loops with an average size of 19.5 nm formed in pure Zr (Fig. 2(a)). In contrast, lower density and smaller a-loops were observed in α -Zr lamellae with lamellae thickness $L=676$ nm (Fig. 2(b)). Moreover, both the density and diameter of a-loops decrease with lamellae thickness ($L=232$ nm and $L=113$ nm), as shown in Figs. 2(c) and (d). This viewing direction is parallel with the prismatic plane ($\bar{1}100$) of the α -Zr lamella, so that the α/β interface is near edge-on.

The density and the size of a-loops in pure Zr and α -Zr lamellae with different lamellae thickness were counted and analysed in Fig. 3. The size of dislocation loop is represented by the diameter of a minimum circle which can totally overlie a single a-loop. The a-loops smaller than 5 nm are excluded in the statistical analysis. As shown in Fig. 3(a), the a-loops areal density are 6.75×10^{14} m⁻² for pure Zr, and 5.81×10^{14} m⁻², 5.13×10^{14} m⁻², 4.64×10^{14} m⁻² for α -Zr lamella with thickness of 676 nm, 232 nm and 113 nm, respectively. It was reported that once foil thickness less than 80 nm [34], the sample surfaces will have a great impact on the defect areal density measurement. However, this effect should be negligible here because α -Zr foils have thickness in the range of 100 nm to 150 nm. During defect characterization, all TEM foils have a homogenous contrast, which indicate that their thickness are similar. Therefore, the defect density measurement is reliable. The size distribution of a-loops in pure Zr and α -Zr lamella are shown in Fig. 3(c-f), and the average size of a-loops are compared in Fig. 3(b). For pure Zr, the average size of a-loops is about 19.5 ± 7.7 nm. By introducing α/β interfaces, the average size of a-loops monotonically reduces as α -Zr lamella thickness decreases. In α -Zr lamella with thickness of 113 nm, the a-loops size show a homogeneous distribution and reduces to 14.6 ± 5.7 nm, which is about three quarters of that in pure Zr. The reduction of

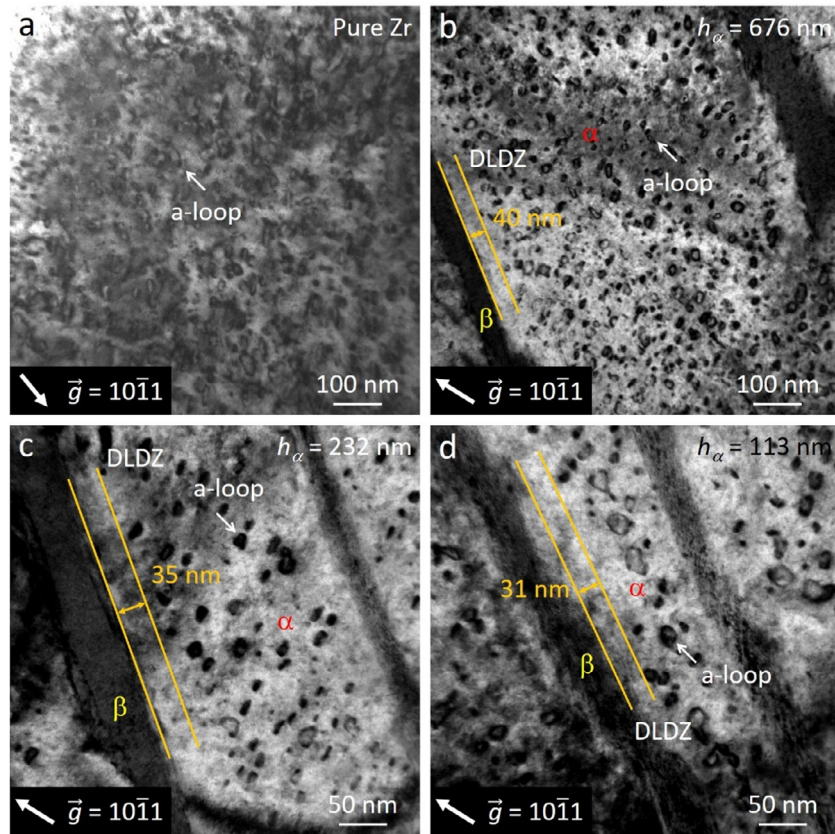


Fig. 2. a-loops in He-irradiated (a) pure Zr, (b-d) DLDZ in α -Zr lamella with thickness of 676 nm, 232 nm and 113 nm.

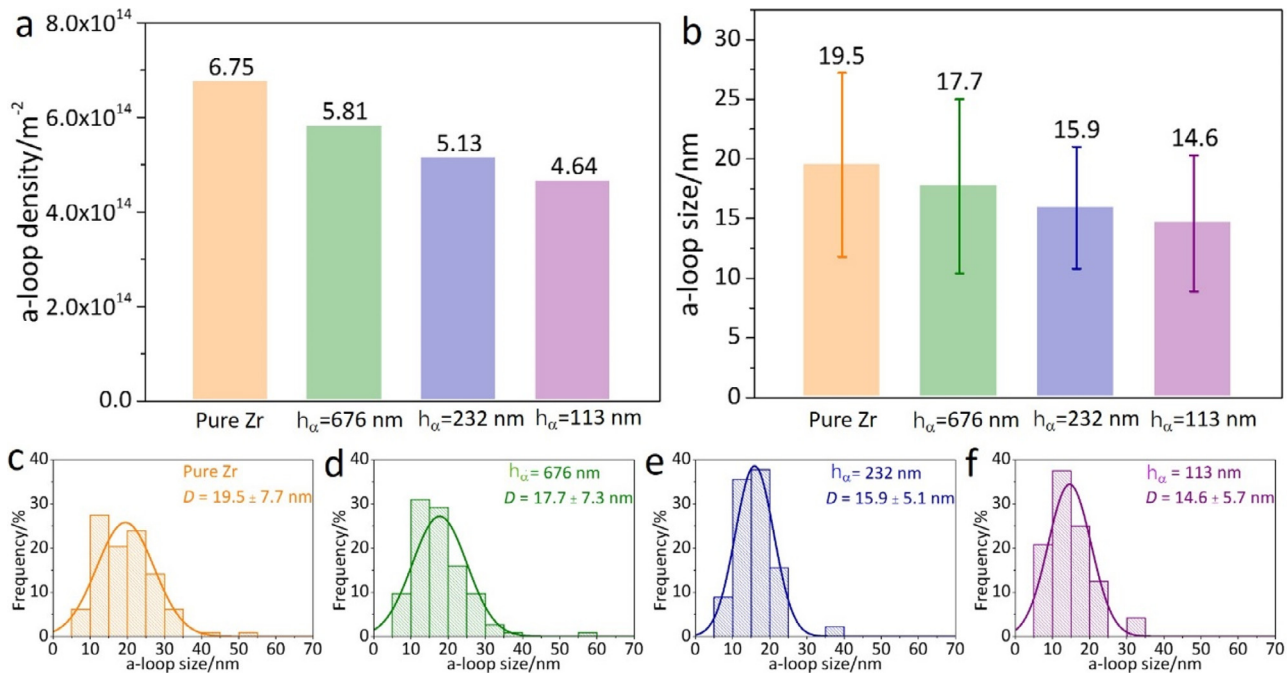


Fig. 3. Statistical plots showing the (a) a-loop density, (b) average size, and (c-f) size distribution of a-loops within pure Zr and α -Zr lamella.

a-loops density and size indicates that higher density of α/β interfaces effectively suppress a-loops nucleation and growth.

Fig. 4 shows the formation of c-loops in nanolayered Zr-2.5Nb after Kr ion irradiation. Profuse line contrast are formed in the α -Zr lamella, indicating high density of c-loops are produced after irradiation to 20 dpa [11]. It is obvious that the number density and

size of c-loops are much smaller in the narrower α -Zr layer with thickness of 152 nm (Fig. 4(c)) compared to that in the Fig. 4(b) with thickness of 531 nm and in pure Zr [11]. This observations show that higher density of α/β interfaces, fewer c-loops. The α -Zr lamella thickness here is different from that in Fig. 2, because α -Zr lamellae in this sample distribute in a wide range [29]. In ad-

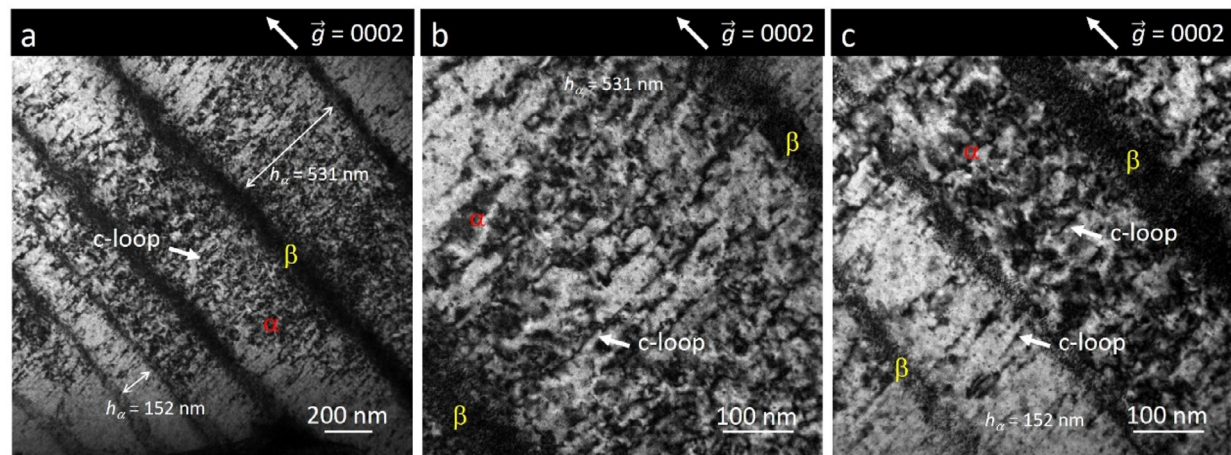


Fig. 4. c-loops in Kr irradiated (20 dpa) α -Zr lamella. (a) Low magnification image; (b) α -Zr layer with thickness of 531 nm; (c) α -Zr layer with thickness of 152 nm.

dition, Kr ion irradiation has much faster dose rate than the He ion implantation. Under similar irradiation condition, faster dose rate induces higher point defect production rate and shorter time for point defect clustering. The effect of α/β interfaces on radiation defect accumulation will be more obvious under smaller dose rates irradiation.

The simultaneous reduction of a-loops and c-loops density and size can be attributed to the influence of α/β interfaces. Both interstitials and vacancies are attracted by the α/β interfaces, thus the annihilation rate of interstitial-vacancy is enhanced, leaving a DLDZ with width from 30 to 40 nm in the vicinity of α/β interface, as shown in Figs. 2(b)-(d). Analogous to void denuded zone produced near Cu/Nb interface [20], these DLDZs are a direct evidence of interface healing irradiation defects. Due to reduced point defects concentration, both a-loops and c-loops nucleation and growth processes are delayed and suppressed [16]. Even though the reduction of a-loop density and size is not significant, but if the α -Zr lamella thickness is further refined down to 80 nm, about twice the DLDZ width, a significant suppression of a-loops and c-loops nucleation and growth should be achieved [18–20]. Additionally, under normal dose rate in a nuclear reactor, lower production rate and longer time for diffusion of point defects contribute to more interstitials or vacancies absorption by α/β interface. Thus, a more noticeable suppression on dislocation loops formation can be expected.

A classical “inside-outside” contrast method was also employed to analyse a-loops character, either interstitial or vacancy type, as shown in Fig. 5. Four steps are required to determine the characteristics of dislocation loop [35]. First, determine the Burgers vector, $\pm \frac{1}{3}\vec{a}_1$ ($\vec{a}_1 = [2\bar{1}\bar{1}0]$), $\pm \frac{1}{3}\vec{a}_2$ ($\vec{a}_2 = [\bar{1}2\bar{1}0]$) or $\pm \frac{1}{3}\vec{a}_3$ ($\vec{a}_3 = [\bar{1}\bar{1}20]$), of a-loops by the invisibility criterion. Second, determine the specific direction or sign, “+” or “-”, of Burgers vector by taking two TEM images under “ $+g$ ” and “ $-g$ ” two-beam condition with deviation parameter $s > 0$ into consideration. The a-loops should show “outside” contrast when $(\vec{g} \cdot \vec{b})s > 0$, while “inside” contrast when $(\vec{g} \cdot \vec{b})s < 0$. Third, characterize the habit plane and its normal, \vec{n} , of a-loops by rotating TEM foil. The \vec{n} points upwards in the electron microscope, or towards the electron source. Last, the a-loops should be interstitial type if $\vec{b} \cdot \vec{n} > 0$, and vacancy type if $\vec{b} \cdot \vec{n} < 0$.

To determine the Burgers vector of a-loops in α -Zr lamella, three images were taken near two-beam conditions, $\vec{g} = 1\bar{1}00$, $10\bar{1}1$ and $01\bar{1}1$ with zone axis close to $[11\bar{2}3]$, respectively, as displayed in Figs. 5(a)–(c). According to the invisibility criterion, $\vec{g} \cdot \vec{b} = 0$, a-loops with Burgers vector parallel to \vec{a}_3 , \vec{a}_2 and \vec{a}_1

are invisible in Figs. 5(a), (b) and (c), respectively. In contrast to Fig. 5(c) with $\vec{g} = 01\bar{1}1$, the a-loops marked by blue arrows are extinct in Fig. 5(a), and show “outside” contrast in Fig. 5(d) with $\vec{g} = 0\bar{1}1\bar{1}$, which is the negative of $01\bar{1}1$. Thus, those a-loops have a Burgers vector of $+\frac{1}{3}\vec{a}_3$.

The irradiation-induced dislocation loops can be regarded as a stacking faults forming by inserting (interstitial loops) or withdrawing (vacancy loops) a layer of atoms on a preferred crystallographic plane. On this basis, their Burgers vectors have a component parallel to the normal of habit plane. Therefore, the marked a-loops with Burgers vector of $+\frac{1}{3}\vec{a}_3$ should lie within prismatic plane P_1 : $(01\bar{1}0)$ or P_2 : $(10\bar{1}0)$, as labelled in Fig. 5(e). This is consistent with the morphology of the marked a-loops in Figs. 5 (b) and (c). Under the viewing direction close to $[11\bar{2}3]$, the prismatic plane P_3 has a near edge-on position. If some of a-loops are on P_3 , their trace line should be parallel to the projection of P_3 . However, none of a-loops follow this position. Therefore, all of a-loops in Fig. 5 are on P_1 or P_2 . Fig. 5(e) illustrates the crystal orientation of α -Zr lamella in Fig. 5(d). Both normal of P_1 and P_2 have an obtuse angle with $\vec{b} = +\frac{1}{3}\vec{a}_3$, hence the marked a-loops in Figs. 5 (b) to (d) are vacancy loops.

Usually, interstitial a-loops are the major defects at irradiation temperature below 300°C [7]. Even for pure Zr irradiated at 400°C, 70% of the dislocation loops are still interstitial a-loops [11]. However, vacancy a-loops are dominated in the current sample, indicating α/β interfaces have a marked effect on the variant of irradiation defects. Irradiation induced self-interstitials diffuse faster and are easily absorbed by the α/β interface. The lack of interstitials inside α -Zr lamella results in lower density and small size of interstitial a-loops. In addition, vacancies also have high mobility at 400°C, and can be absorbed by the α/β interfaces. Therefore, vacancy concentration in nanoscale α -Zr lamella is lower than that in pure Zr, which leads to fewer and smaller vacancy a-loops. This is also the mechanism for the fewer and smaller c-loops in narrow α -Zr lamella observed in Fig. 4(c). Simultaneously, the interstitial-vacancy recombination is accelerated in the vicinity of α/β interface, which produce a DLDZ in the adjacent of interface. Due to the enhanced annihilation and lower density of point defects inside α -Zr lamella, the nucleation and growth of a-loops and c-loops can be effectively suppressed by the high density of α/β interfaces.

In summary, we characterized the a-loops and c-loops in ions irradiated nanolayered Zr-2.5Nb. High density of α/β interfaces effectively reduces the formation of a-loops and c-loops. Numerous α/β interfaces act as efficient sinks for irradiation-induced point defects, facilitate the recombination of irradiation induced intersti-

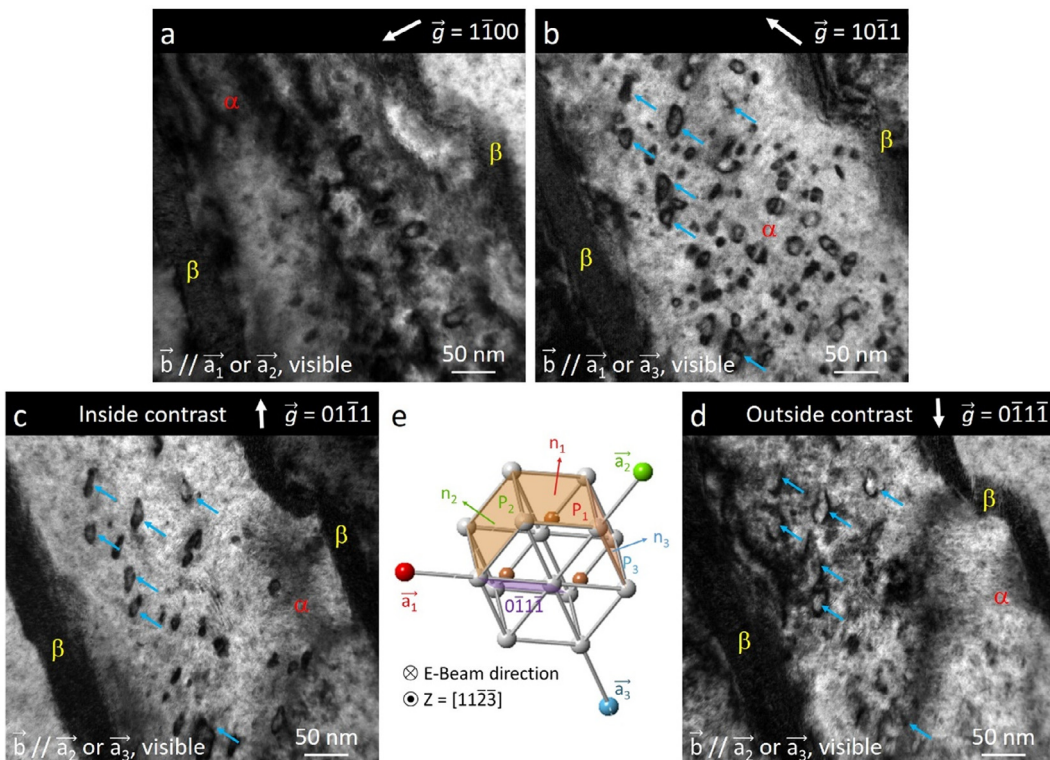


Fig. 5. Determination of a-loops characteristic using the “inside-outside” contrast method. (a-c) Analysis of a-loops Burgers vector by invisibility criterion, $\vec{g} \cdot \vec{b} = 0$. (d) The a-loops marked by blue arrows show an “outside” contrast, compared with (c). (e) The orientation of crystal for α -Zr lamella in (d).

tials and vacancies, thus enhance irradiation resistance, and make hierarchical 3D nanolayered Zr-2.5Nb alloy a promising structural material for extreme environments.

Declaration of Competing Interest

The authors declare that there is no conflict of interest.

Acknowledgements

This work was supported by the National Natural Science Foundation of China (Grant Nos. 51922082 and 51971170), the 111 Project of China (Grant Number BP2018008) and the Innovation Project of Shaanxi Province (Grant No. 2017KTPPT-12). J.W.Z appreciates X.W.Z and R.Y.Z. for assistance in experiments.

References

- [1] R.A. Holt, J. Nucl. Mater. 372 (2008) 182–214.
- [2] R. Tewari, D. Srivastava, G.K. Dey, J.K. Chakravarty, S. Banerjee, J. Nucl. Mater. 383 (2008) 153–171.
- [3] M. Griffiths, J. Nucl. Mater. 159 (1988) 190–218.
- [4] M. Topping, A. Harte, T. Ungár, C.P. Race, S. Dumbill, P. Frankel, M. Preuss, J. Nucl. Mater. 514 (2019) 358–367.
- [5] C.G. Yan, R.S. Wang, Y.L. Wang, X.T. Wang, G.G. Bai, Nucl. Eng. Technol. 47 (2015) 323–331.
- [6] H.B. Yu, Z.W. Yao, Y. Idrees, H.K. Zhang, M.A. Kirk, M.R. Daymond, J. Nucl. Mater. 491 (2017) 232–241.
- [7] A. Jostsons, P.M. Kelly, R.G. Blake, J. Nucl. Mater. 66 (1977) 236–256.
- [8] M. Griffiths, R.W. Gilbert, C.E. Coleman, J. Nucl. Mater. 159 (1988) 405–416.
- [9] E. Francis, R.P. Babu, A. Harte, T.L. Martin, P. Frankel, D. Jadernas, J. Romero, L. Hallstadius, P.A.J. Bagot, M.P. Moody, M. Preuss, Acta Mater. 165 (2019) 603–614.
- [10] S. Yamada, T. Kameyama, J. Nucl. Mater. 422 (2012) 167–172.
- [11] S.M. Liu, I.J. Beyerlein, W.Z. Han, Nat. Commun. 11 (2020) 5766.
- [12] F. Long, L. Balogh, D.W. Brown, P. Mosbrucker, T. Skippon, C.D. Judge, M.R. Daymond, Acta Mater. 102 (2016) 352–363.
- [13] B. Christiaen, C. Domain, L. Thuinet, A. Ambard, A. Legris, Acta Mater. 195 (2020) 631–644.
- [14] R.B. Adamson, C.E. Coleman, M. Griffiths, J. Nucl. Mater. 521 (2019) 167–244.
- [15] M. Christensen, W. Wolf, C. Freeman, E. Wimmer, R.B. Adamson, M. Griffiths, E.V. Mader, J. Nucl. Mater. 529 (2020) 151946.
- [16] W.Z. Han, M.J. Demkowicz, E.G. Fu, Y.Q. Wang, A. Misra, Acta Mater. 60 (2012) 6341–6351.
- [17] X.H. Zhang, K. Hattar, Y.X. Chen, L. Shao, J. Li, C. Sun, K.Y. Yu, N. Li, M.L. Taheri, H.Y. Wang, J. Wang, M. Nastasi, Prog. Mater. Sci. 96 (2018) 217–321.
- [18] M. Wang, I.J. Beyerlein, J. Zhang, W.Z. Han, Acta Mater. 160 (2018) 211–223.
- [19] M. Wang, I.J. Beyerlein, J. Zhang, W.Z. Han, Scr. Mater. 171 (2019) 1–5.
- [20] W.Z. Han, M.J. Demkowicz, N.A. Mara, E.G. Fu, S. Sinha, A.D. Rollett, Y.Q. Wang, J.S. Carpenter, I.J. Beyerlein, A. Misra, Adv. Mater. 25 (2013) 6975–6979.
- [21] O. El-Atwani, J.E. Nathaniel, A.C. Leff, J.K. Baldwin, K. Hattar, M.L. Taheri, Mater. Res. Lett. 5 (2017) 195–200.
- [22] G. Ackland, Science 327 (2010) 1587–1588.
- [23] X.M. Bai, A.F. Voter, R.G. Hoagland, M. Nastasi, B.P. Uberuaga, Science 327 (2010) 1631–1634.
- [24] M. Callisti, T. Polcar, Acta Mater. 124 (2017) 247–260.
- [25] M. Callisti, M. Karlik, T. Polcar, Scr. Mater. 152 (2018) 31–35.
- [26] J.S. Carpenter, T. Nizolek, R.J. McCabe, M. Knezevic, S.J. Zheng, B.P. Eftink, J.E. Scott, S.C. Vogel, T.M. Pollock, N.A. Mara, I.J. Beyerlein, Acta Mater. 92 (2015) 97–108.
- [27] M. Knezevic, T. Nizolek, M. Ardeljan, I.J. Beyerlein, N.A. Mara, T.M. Pollock, Int. J. Plast. 57 (2014) 16–28.
- [28] W.Z. Han, E.G. Fu, M.J. Demkowicz, Y.Q. Wang, A. Misra, J. Mater. Res. 28 (2013) 2763–2770.
- [29] J.W. Zhang, I.J. Beyerlein, W.Z. Han, Phys. Rev. Lett. 122 (2019) 255501.
- [30] X.W. Zou, J.W. Zhang, W.Z. Han, J. Mater. Res. (2021).
- [31] R.M. Hengstler-Eger, P. Baldo, L. Beck, J. Dorner, K. Ertl, P.B. Hoffmann, C. Hugenschmidt, M.A. Kirk, W. Petry, P. Pikart, A. Rempel, J. Nucl. Mater. 423 (2012) 170–182.
- [32] N. Gharbi, F. Onimus, D. Gilbon, J.P. Mardon, X. Feaugas, J. Nucl. Mater. 467 (2015) 785–801.
- [33] Y. Idrees, Z. Yao, M.A. Kirk, M.R. Daymond, J. Nucl. Mater. 433 (2013) 95–107.
- [34] D.H. Xu, B.D. Wirth, M.M. Li, M.A. Kirk, Acta Mater. 60 (2012) 4286–4302.
- [35] H. Foll, M. Wilkens, Phys. Stat. Sol. (a) 31 (1975) 519–524.